RESEARCH ARTICLE

A hierarchical anatomical framework and workflow for organizing stereotactic encephalography in epilepsy

Bryan Zheng[1] | Ben Hsieh[2] | Nathaniel Rex[2] | Peter M. Lauro[1] | Scott A. Collins[2] | Andrew S. Blum[3] | Julie L. Roth[3] | Neishay Ayub[3] | Wael F. Asaad[1]

[1]Department of Neurosurgery, Warren Alpert Medical School, Brown University, Providence, Rhode Island, USA

[2]Department of Diagnostic Imaging, Warren Alpert Medical School, Brown University, Providence, Rhode Island, USA

[3]Department of Neurology, Warren Alpert Medical School, Brown University, Providence, Rhode Island, USA

Correspondence
Bryan Zheng, Department of Neurosurgery, Warren Alpert Medical School, Brown University, Providence, RI 02903, USA.
Email: bryan_zheng@brown.edu

Abstract

Stereotactic electroencephalography (SEEG) is an increasingly utilized method for invasive monitoring in patients with medically intractable epilepsy. Yet, the lack of standardization for labeling electrodes hinders communication among clinicians. A rational clustering of contacts based on anatomy rather than arbitrary physical leads may help clinical neurophysiologists interpret seizure networks. We identified SEEG electrodes on post-implant CTs and registered them to preoperative MRIs segmented according to an anatomical atlas. Individual contacts were automatically assigned to anatomical areas independent of lead. These contacts were then organized using a hierarchical anatomical schema for display and interpretation. Bipolar-referenced signal cross-correlations were used to compare the similarity of grouped signals within a conventional montage versus this anatomical montage. As a result, we developed a hierarchical organization for SEEG contacts using well-accepted, free software that is based solely on their post-implant anatomical location. When applied to three example SEEG cases for epilepsy, clusters of contacts that were anatomically related collapsed into standardized groups. Qualitatively, seizure events organized using this framework were better visually clustered compared to conventional schemes. Quantitatively, signals grouped by anatomical region were more similar to each other than electrode-based groups as measured by Pearson correlation. Further, we uploaded visualizations of SEEG reconstructions into the electronic medical record, rendering them durably useful given the interpretable electrode labels. In conclusion, we demonstrate a standardized, anatomically grounded approach to the organization of SEEG neuroimaging and electrophysiology data that may enable improved communication among and across surgical epilepsy teams and promote a clearer view of individual seizure networks.

1 | INTRODUCTION

Of the approximately 50 million people with epilepsy worldwide, around one-third of cases are resistant to medication (GBD 2016 Brain and Other CNS Cancer Collaborators, 2019; Kwan & Brodie, 2000; Picot et al., 2008; Sander, 1993). These patients should be evaluated for epilepsy surgery if amenable, which can include resection or ablation of the seizure focus, or neuromodulation of the seizure network. If they undergo one of these operations, the degree of postoperative seizure control is heavily dependent on identification and disablement of the epileptogenic zone (Englot et al., 2012, 2013; Jobst & Cascino, 2015).

Noninvasive diagnostic measures for characterizing seizure networks can include magnetic resonance imaging (MRI), surface electroencephalography (EEG), positron emission tomography (PET), magnetoencephalography (MEG), and neuropsychological evaluations. However, patients may elect to undergo invasive monitoring if clinical data do not converge on a clear seizure source to address surgically (Diehl & Luders, 2000; Sarikaya, 2015). The two primary methods for intracranial recordings are via stereotactic(stereo)-EEG (SEEG) depth electrodes and subdural electrode grids and strips. The advantages and disadvantages of each have been extensively studied, reported, and reviewed (Podkorytova et al., 2016). Though the factors influencing the choice between these two procedures are complex, it is now generally well-accepted that SEEG entails fewer complications while enabling access to more brain regions for exploration (Mullin et al., 2016; Podkorytova et al., 2016; Taussig et al., 2020).

However, whereas subdural grids have the advantage of a regular arrangement of electrodes such that the relationships of signals across contacts have an intuitive spatial order, SEEG depth electrode placement can be highly variable in trajectory, contact geometry, and lead spacing. To mitigate this, some groups have advocated for the use of orthogonal lead placements and "typical" trajectories (Bourdillon et al., 2018; Faraji et al., 2020; Khoo et al., 2020). Others, meanwhile, have created labeling algorithms to standardize SEEG nomenclature based upon lead trajectories (Stone et al., 2020). Unfortunately, the former approach may constrain the use of SEEG in a flexible and patient-specific manner, while the proposed labeling schemes are rather complex and unintuitive, limiting widespread adoption. Furthermore, these approaches tend to ignore the problem of organizing the display of signals in a manner that is sufficiently consistent across cases to allow the development of some visual intuition for interpretation, yet flexible enough to enable application across widely varying implant strategies.

To address these limitations, we propose a framework that is built up from the "ground truth" of brain anatomy and abstracted from the arbitrary details of implant technology. In other words, rather than treating the lead that carries electrodes as the basic unit of neurophysiology, as is currently done with existing nomenclatures and typical montages, we consider individual contacts independently of the leads that support them and assign contact labels and relative organization based upon a rational, hierarchical anatomical schema.

We demonstrate this approach by building a pipeline for organizing SEEG imaging and electrophysiological data using well-accepted, free neuroimaging tools and clinically indicated images. By adapting a standard atlas, our approach applies hierarchical labeling of SEEG contacts abstracted from the arbitrary constraints of the physical leads (Jung et al., 2021; Reveley et al., 2017). As a simple example of the flavor of this approach, one can appreciate that the deeper (more distal) contacts on a series of depth leads targeting the medial temporal lobe are likely more electrographically similar to each other than with the more proximal contacts that target the lateral temporal lobe. Thus, grouping contacts as medial versus lateral may be preferred over grouping them according to the leads on which they reside. Further, those lateral contacts may be best viewed as clustered according to gyrus as well as anterior–posterior position, especially when SEEG lead density is high. This general approach can be combined with existing brain parcellation software to cluster and label contacts based on patient-specific anatomy down to the gyrus, sulcus, or nucleus (Desikan et al., 2006; Destrieux et al., 2010). In addition, we argue that exporting final products of this parcellation, incorporating broadly understood anatomical labels, to the electronic medical record (EMR) can improve communication among the clinical team by allowing all individuals to view the results of this approach without the need for familiarity with specialized software used to create those results.

2 | MATERIALS AND METHODS

The minimum subject-specific image sequences needed include preoperative T1-weighted MRI and postoperative computed tomography (CT) of the brain, which are both already obtained for the routine clinical course (Figure 1). Though not strictly required, the surgical plan of electrode trajectories is extremely helpful for identifying electrodes on imaging, particularly in complex explorations. While we generate and illustrate each component using common and accessible research and clinical software, this general pipeline is well-established and the precise tools used to achieve any step may be adapted based on institutional preference.

During data exportation and prior to any processing, image sequences were anonymized to maintain strict patient privacy in accordance with the Health Insurance Portability and Accountability Act (HIPAA) and the local Institutional Review Board (IRB #217972).

2.1 | CT/MRI registration

In order to ultimately associate contacts, which can be visualized using high-resolution post-implantation CT, with an anatomical location, they must be transformed into the same space as the reference preoperative
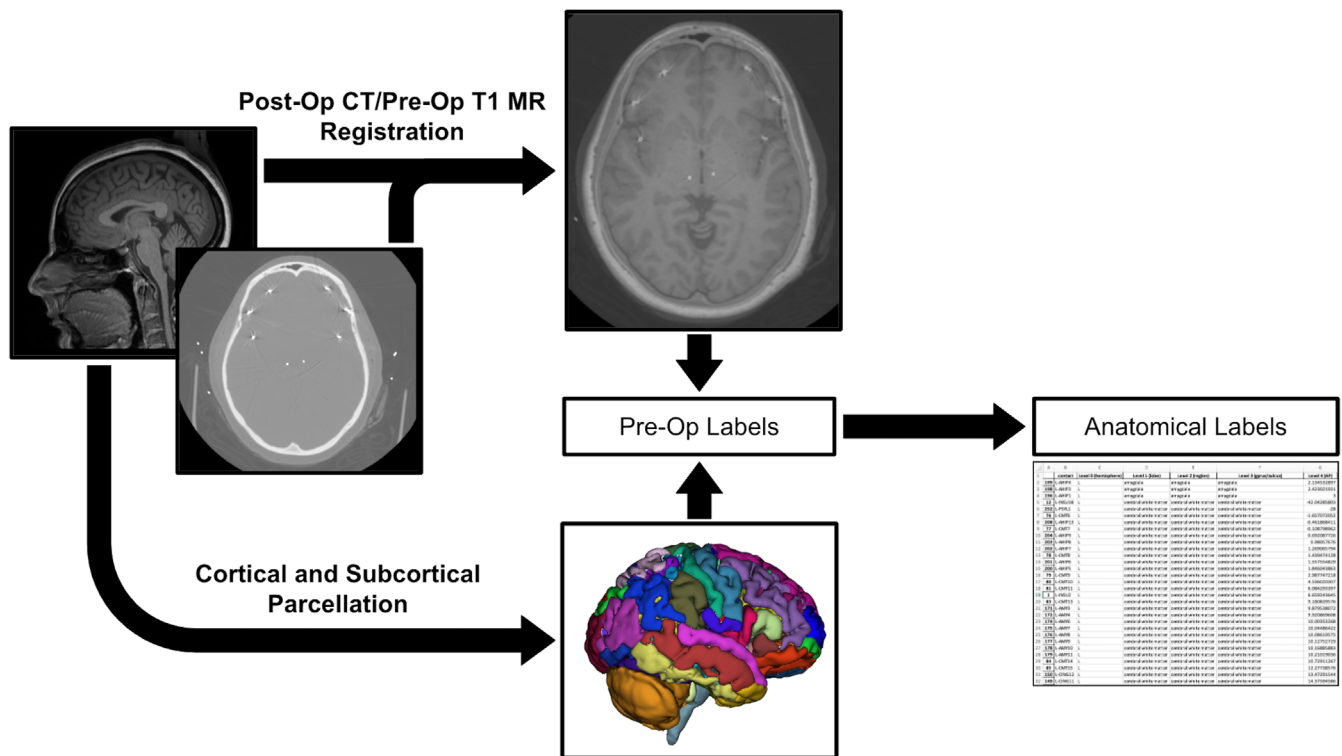
FIGURE 1 General schematic for generating anatomical electrode labels. The segmented T1-weighted MR is used to bridge electrodes seen on postoperative CT to patient anatomy-space. The final output of this imaging pipeline is a re-organized hierarchical spreadsheet of contacts that associates preoperative labels with a new abstracted one.

MRI. We used a step-wise process starting within the surgical planning software used to draft depth electrode trajectories (Waypoint Navigator, *v4.6, FHC*). First, we registered the preoperative MRI to a preoperative CT angiograph (CTA) via an automatic nonrigid algorithm, then registered the postoperative CT to the preoperative CTA, transitively transforming the preoperative MRI to postoperative CT space.

2.2 | Brain parcellation

Our labeling scheme relies on automatic segmentation of cortical and subcortical regions of interest for each patient. We implemented the *recon_all* function in FreeSurfer v7.1.0 (*Athinoula A. Martinos Center for Biomedical Imaging*) to accomplish this step. Importantly, the Desikan-Killiany (DK) atlas incorporated in FreeSurfer is already roughly hierarchically organized and can therefore be easily adapted generally to compile the final tree of labels. Modifications to the DK atlas, namely to segment amygdaloid and hippocampal subfields, thalamic nuclei, and insular gyri, were made using the Destreiux cortical atlas in FreeSurfer and other incorporated atlases (Destrieux et al., 2010; Fischl et al., 2004; Iglesias et al., 2015, 2016, 2018; Saygin et al., 2017).

2.3 | Contact segmentation

Each depth electrode is assigned a unique label, based on the electrode target. Each electrode contact along the depth electrode is assigned a number based on physical location along the lead, usually ascending deep-to-superficial. Indeed, these labels are typically used for all further communication and conceptualization of neurophysiological data. Further, these labels are also usually used by the clinical electrophysiology software for organizing EEG montages, which are subsequently interpreted by a neurologist.

Electrodes seen on postoperative CT can be identified using the intended trajectories from the surgical plan. We then used *3DSlicer* (*v4.11, Brigham and Women's Hospital*) markups to reconstruct models of each electrode based on specifications from the electrode manufacturer (MICRODEEP Depth Electrodes, DIXI Medical), giving each contact name a coordinate in the CT/MR/Parcellation space (Fedorov et al., 2012). Using the Python interface in *3DSlicer*, we automatically generate a list of each contact with its coordinates and location within the segmented brain, which can be grouped hierarchically based on anatomy.

2.4 | Neurophysiological montages

Signals were lowpass filtered using a second-order Butterworth filter (cutoff frequency = 200 Hz). For visualization, signals were displayed as a montage using a bipolar referencing scheme, subtracting the adjacent superficial signal from each contact, as is common in clinical practice. Signals were manually inspected and those with significant artifact were excluded from the analysis. Of note, contacts located in white matter but that were within 2 mm of a gray matter segment

TABLE 1 Hierarchical classification scheme for SEEG depth leads

FreeSurfer label	Level 1: lobe	Level 2: region	Level 3: gyrus/nucleus	Location	Coordinate preference
Lateral-nucleus	Temporal	Medial	Amygdala: lateral nucleus	Lateral nucleus	ap
Basal-nucleus	Temporal	Medial	Amygdala: basal nucleus	Basal nucleus	ap
Central-nucleus	Temporal	Medial	Amygdala: central nucleus	Central nucleus	ap
Medial-nucleus	Temporal	Medial	Amygdala: medial nucleus	Medial nucleus	ap
Cortical-nucleus	Temporal	Medial	Amygdala: cortical nucleus	Cortical nucleus	ap
Accessory-basal-nucleus	Temporal	Medial	Amygdala: accessory basal nucleus	Accessory basal nucleus	ap
Corticoamygdaloid-transitio	Temporal	Medial	Amygdala: corticoamygdaloid transition	Corticoamygdaloid transition	ap
Anterior-amygdaloid-area-AAA	Temporal	Medial	Amygdala: anterior area	Anterior amygdaloid area	ap
Paralaminar-nucleus	Temporal	Medial	Amygdala: paralaminar nucleus	Paralaminar nucleus	ap
Amygdala	Temporal	Medial	Amygdala	Amygdaloid unknown	ap
Parasubiculum	Temporal	Medial	Hippocampus: parasubiculum	Parasubiculum	ap
Presubiculum	Temporal	Medial	Hippocampus:presubiculum	Presubiculum	ap
Subiculum	Temporal	Medial	Hippocampus: subiculum	Subiculum	ap
CA1	Temporal	Medial	Hippocampus: CA1	CA1	ap
CA3	Temporal	Medial	Hippocampus: CA3	CA3	ap
CA4	Temporal	Medial	Hippocampus: CA4	CA4	ap
GC-DG	Temporal	Medial	Hippocampus: dentate gyrus	Dentate gyrus	ap
HATA	Temporal	Medial	Hippocampus: HATA	Hippocampal amygdala transition area	ap
Fimbria	Temporal	Medial	Hippocampus: fimbria	Fimbria	ap
Molecular_layer_HP	Temporal	Medial	Hippocampus: molecular layer	Hippocampal molecular layer	ap
Hippocampal_fissure	Temporal	Medial	Hippocampus: fissure	Hippocampal fissure	ap
HP_tail	Temporal	Medial	Hippocampus: tail	Hippocampal tail	ap
Hippocampus	Temporal	Medial	Hippocampus	Hippocampal unknown	ap
Entorhinal	Temporal	Medial	Entorhinal cortex	Entorhinal cortex	ap
Parahippocampal	Temporal	Medial	Parahippocampal gyrus	Parahippocampal gyrus	ap
Temporalpole	Temporal	Medial	Temporal pole	Temporal pole	ap
Fusiform	Temporal	Medial	Fusiform gyrus	Fusiform gyrus	ap
Superiortemporal	Temporal	Lateral	Superior temporal gyrus	Superior temporal gyrus	ap
Middletemporal	Temporal	Lateral	Middle temporal gyrus	Middle temporal gyrus	ap
Inferiortemporal	Temporal	Lateral	Inferior temporal gyrus	Inferior temporal gyrus	ap
Transversetemporal	Temporal	Lateral	Transverse temporal cortex	Transverse temporal cortex	ap
Frontalpole	Frontal	Anterior	Frontal pole	Frontal pole	ap
Superiorfrontal	Frontal	Superior	Superior frontal gyrus	Superior frontal gyrus	ap
Rostralmiddlefrontal	Frontal	Middle	Middle frontal gyrus	Rostral middle frontal gyrus	ap
Caudalmiddlefrontal	Frontal	Middle	Middle frontal gyrus	Caudal middle frontal gyrus	ap
Parsopercularis	Frontal	Inferior	Inferior frontal gyrus	Pars opercularis	ap
Parstriangularis	Frontal	Inferior	Inferior frontal gyrus	Pars triangularis	ap
Parsorbitalis	Frontal	Inferior	Inferior frontal gyrus	Pars orbitalis	ap
Medialorbitofrontal	Frontal	Orbitofrontal	Orbitofrontal cortex	Medial orbitofrontal cortex	ap
Lateralorbitofrontal	Frontal	Orbitofrontal	Orbitofrontal cortex	Lateral orbitofrontal cortex	ap

TABLE 1 (Continued)

FreeSurfer label	Level 1: lobe	Level 2: region	Level 3: gyrus/nucleus	Location	Coordinate preference
Paracentral	Frontal	Central	Paracentral lobule	Paracentral lobule	ap
Precentral	Frontal	Central	Precentral gyrus	Precentral gyrus	si
Insular_short	Insula	Short	Insula: short gyri	Short insular gyri	si
Ins_lg_and_S_cent_ins	Insula	Long	Insula: long gyri	Long insular gyri	si
Circular_insula_ant	Insula	Circular	Insula: anterior circular sulcus	Anterior circular insular sulcus	si
Circular_insula_inf	Insula	Circular	Insula: inferior circular sulcus	Inferior circular insular sulcus	ap
Circular_insula_sup	Insula	Circular	Insula: superior circular sulcus	Superior circular insular sulcus	ap
Insula	Insula	Other	Insula	Insular unknown	ap
Postcentral	Parietal	Central	Postcentral gyrus	Postcentral gyrus	si
Superiorparietal	Parietal	Superior	Superior parietal cortex	Superior parietal cortex	ap
Inferiorparietal	Parietal	Inferior	Inferior parietal cortex	Inferior parietal cortex	ap
Supramarginal	Parietal	Inferior	Supramarginal gyrus	Supramarginal gyrus	ap
Precuneus	Parietal	Medial	Precuneus cortex	Precuneus cortex	ap
Rostralanteriorcingulate	Cingulate	Anterior	Anterior cingulate cortex	Rostral anterior cingulate cortex	ap
Caudalanteriorcingulate	Cingulate	Anterior	Anterior cingulate cortex	Caudal anterior cingulate cortex	ap
Posteriorcingulate	Cingulate	Posterior	Posterior cingulate cortex	Posterior cingulate cortex	ap
Isthmuscingulate	Cingulate	Inferior	Isthmus of cingulate gyrus	Isthmus of cingulate gyrus	ap
Corpuscallosum	Cingulate	Inferior	Corpus callosum	Corpus callosum	ap
Cuneus	Occipital	Medial	Cuneus cortex	Cuneus cortex	ap
Pericalcarine	Occipital	Medial	Pericalcarine cortex	pericalcarine cortex	ap
Lingual	Occipital	Medial	Lingual cyrus	Lingual cyrus	ap
Lateraloccipital	Occipital	Lateral	Lateral occipital cortex	Lateral occipital cortex	ap
AV	Thalamus	Anterior	Thalamus:AV nucleus	Anteroventral nucleus	ap
LD	Thalamus	Lateral	Thalamus:LD nucleus	Laterodorsal nucleus	ap
LP	Thalamus	Lateral	Thalamus:LP nucleus	Lateral posterior nucleus	ap
VA	Thalamus	Ventral	Thalamus:VA nucleus	Ventral anterior nucleus	ap
VAmc	Thalamus	Ventral	Thalamus:VA magnocellular nucleus	Ventral anterior magnocellular nucleus	ap
Vla	Thalamus	Ventral	Thalamus:VLa nucleus	Ventral lateral anterior nucleus	ap
VLp	Thalamus	Ventral	Thalamus:VLp nucleus	Ventral lateral posterior nucleus	ap
VPL	Thalamus	Ventral	Thalamus:VPL nucleus	Ventral posterolateral nucleus	ap
VM	Thalamus	Ventral	Thalamus:VM nucleus	Ventromedial nucleus	ap
CeM	Thalamus	Intralaminar	Thalamus:CeM nucleus	Central medial nucleus	ap
CL	Thalamus	Intralaminar	Thalamus:CL nucleus	Central lateral nucleus	ap
Pc	Thalamus	Intralaminar	Thalamus:Pc nucleus	Paracentral nucleus	ap
CM	Thalamus	Intralaminar	Thalamus:CM nucleus	centromedian nucleus	ap
Pf	Thalamus	Intralaminar	Thalamus:Pf nucleus	Parafascicular nucleus	ap
Pt	Thalamus	Medial	Thalamus:Pt nucleus	Paratenial nucleus	ap
MV-re	Thalamus	Medial	Thalamus:reuniens nucleus	Reuniens nucleus	ap
MDm	Thalamus	Medial	Thalamus:MDm nucleus	Mediodorsal medial magnocellular nucleus	ap

TABLE 1 (Continued)

FreeSurfer label	Level 1: lobe	Level 2: region	Level 3: gyrus/nucleus	Location	Coordinate preference
MDl	Thalamus	Medial	Thalamus:MDl nucleus	Mediodorsal lateral parvocellular nucleus	ap
LGN	Thalamus	Posterior	Thalamus:LGN	Lateral geniculate nucleus	ap
MGN	Thalamus	Posterior	Thalamus:MGN	Medial geniculate nucleus	ap
L-Sg	Thalamus	Posterior	Thalamus:limitans	Limitans	ap
PuA	Thalamus	Posterior	Thalamus:PuA nucleus	Anterior pulvinar nucleus	ap
PuM	Thalamus	Posterior	Thalamus:PuM nucleus	Medial pulvinar nucleus	ap
PuL	Thalamus	Posterior	Thalamus:PuL nucleus	Lateral pulvinar nucleus	ap
PuI	Thalamus	Posterior	Thalamus:PuI nucleus	Inferior pulvinar nucleus	ap
R	Thalamus	Other	Thalamus:TRN	Thalamic reticular nucleus	ap
Thalamus	Thalamus	Other	Thalamus	Thalamic unknown	ap
Caudate	Basal ganglia	Striatum	Caudate nucleus	Caudate nucleus	ap
Putamen	Basal ganglia	Striatum	Putamen	Putamen	ap
Cerebral-White-Matter	White matter	White matter	White matter	White matter	ap
CSF	csf	csf	csf	csf	ap
Hypointensities	Hypointensities	Hypointensities	Hypointensities	Hypointensities	ap
Unknown	Unknown	Unknown	Unknown	Unknown	ap

were included in that segment but were marked as exceptions. Remaining white matter contacts were positioned at the bottom of the anatomical montages. Clinical EEG interpretations were reviewed for contacts or electrode regions (e.g., deep or superficial) that were noted to be involved in a particular seizure.

Signal similarity was assessed using the average Pearson product–moment correlation coefficients (r) for contacts grouped by anatomical regions and by physical lead. In order to mitigate the effects of co-dependencies between signals caused by bipolar referencing, an average "group signal" was calculated for every anatomical segment and physical electrode. Then, each signal used to obtain the mean signal was correlated to it, resulting in a distribution of r values based on each signal under the anatomical and conventional schemes. An independent two-tailed t-test was used to assess for differences in mean Pearson correlations within fundamental units of the anatomical (segmented regions) versus conventional (depth electrodes) montages (*v3.8, Python Software Foundation*).

3 | RESULTS

3.1 | Hierarchical framework

We first constructed a hierarchical classification of brain regions based upon the labels extracted from an adapted DK human brain atlas (Table 1). For cortical regions, the hierarchy was built up from gyrus to lobe to hemisphere (Figure 2). Priority was given for sites within a single gyrus assigned anterior before posterior, as the principal axis for several frequently sampled regions (e.g., hippocampus,

superior/middle/inferior temporal gyri) is most parallel to that axis. Exceptions were made for the few gyri such as the motor and sensory cortices whose major axes run inferiorly, in which case priority was given to superior sites. For subcortical structures, the hierarchy was built up from nucleus to nuclear group to hemisphere, with the same Cartesian preferences for location within a nucleus. An implicit "zeroth" level denotes the hemisphere of the contact coordinates.

3.2 | Illustrative cases

The hierarchical labeling scheme was then applied to three patients with medically intractable epilepsy who underwent SEEG explorations at our institution. Characterization of each subject and their epilepsies is outlined in Table 2. We registered each preoperative T1 MRI to a high-resolution postoperative CT. After cortical segmentation, all contacts were then associated with their preoperative label and modeled in *3DSlicer*. The coordinates of each contact were then used to associate each contact with a region of interest as defined by the patient-specific brain parcellation. Finally, our framework was applied to this list to automatically reorganize the list of contacts from preoperative physical leads to a spreadsheet organized by an anatomically based hierarchy. The relabeled contacts were applied and overlayed on the CT-MRI registrations for end-user visualization. At this point, leads are associated with known anatomy and consequently can be generally understood. Reconstructions may therefore be uploaded to the standard picture archiving and communication systems (PACS) as a permanent part of the patient's EMR to aid in all future clinical assessments.

FIGURE 2 Generalized cortical and subcortical segmentation hierarchies. Both cortical (left) and subcortical (right) segmentations follow parallel hierarchies, beginning with hemisphere and ending with specific gyri and nuclei, respectively. Once contacts are grouped at the final level, they can be ordered based on the principal axis of the gyrus or nucleus.
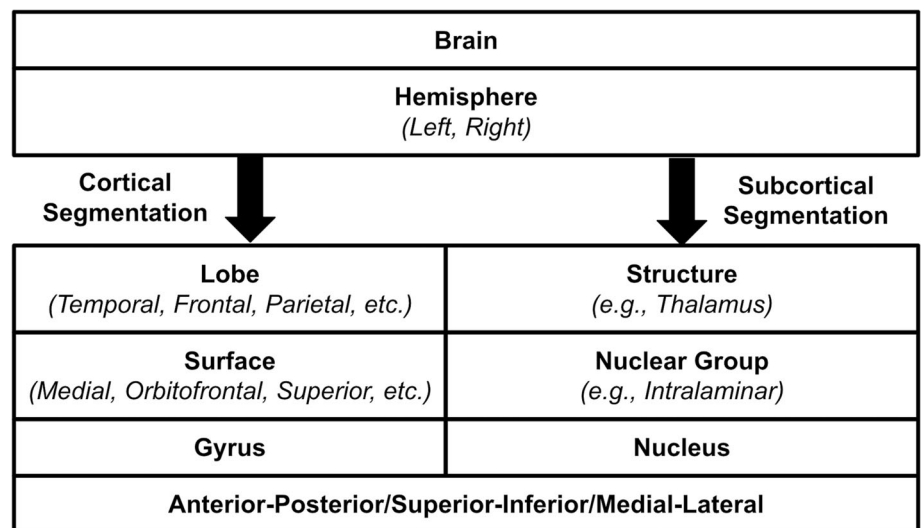

TABLE 2 Characterization of patient epilepsies from illustrative examples

	Patient 1	Patient 2	Patient 3
Sex	Female	Female	Female
Age of Onset (years)	Childhood	20	*1st semiology*: 6 *2nd semiology*: 25
Duration (years)	~20	16	19
Seizure type	FBTC	FIAS; FBTC	FA, FA (both semiologies)
Semiology	Left head/gaze deviation, left facial twitching, left hand clenching, followed by secondary generalization	Behavioral arrest with oral and manual automatisms, followed by secondary generalizations	*1st semiology*: Left sided clonic activity (controlled) *2nd semiology*: Brief events of left head version with bilateral LE adduction and/or RLE elevation
Frequency	2–3/month	4/month	*1st semiology*: None currently *2nd semiology*: 1–3/day
MRI findings	R hemispheric atrophy, R MTS, corpus callosum hypoplasia, L parietal VP shunt	Normal	Multiple GM heterotopias, bilateral Perisylvian polymicrogyria, callosal dysgenisias, focal cortical dysplasias
PET findings	Not obtained	Small subtle area of mild asymmetry with decreased activity in the left anterolateral temporal lobe	Mild asymmetric diminished activity in the left mid-tempoparietal region
Localization on phase I monitoring	R frontotemporal	Bitemporal	None
SEEG approach	Right	Bilateral (symmetric)	Bilateral (symmetric)
Depth electrode targets	3 temporal, 6 frontal	6 temporal, 6 frontal, 4 cingulate, 2 opercular, 2 insular, 2 thalamic	4 temporal, 6 frontal, 4 parietal, 4 cingulate, 2 insular, 2 thalamic

Abbreviations: FA, focal aware; FBTC, focal to bilateral tonic clonic; FIAS, focal impaired awareness; GM, gray matter; L, left; LE, lower extremity; MTS, mesial temporal sclerosis; R, right.

To more fully illustrate the clinical utility of this framework, we created montages capturing a seizure from three SEEG cases. By design, clusters of electrodes that were anatomically related collapsed into standardized groups. Consequently, contacts noted to be clinically relevant often cluster, facilitating interpretation of the seizure network. For Subject 1 (Figure 3), the deep contacts of electrodes targeting the amygdala and hippocampus (A-AMY, B-PHIP, C-MHIP) were consistently noted in clinical EEG interpretations of captured seizures, and expectedly aggregated as medial temporal lobe contacts when anatomically organized. Likewise, for Subject 2 (Figure 4), deep contacts targeting the medial temporal lobe clustered together (L-AMYG, L-HIPB, L-HIPH) along with deep contacts on insular (L-PINS) and opercular (L-OPER) electrodes. By segmenting out white matter electrodes and relegating them to the bottom of the montage, the temporal onset and likely spread to the frontal lobe was visually more apparent. Subject 3, who had multiple MRI
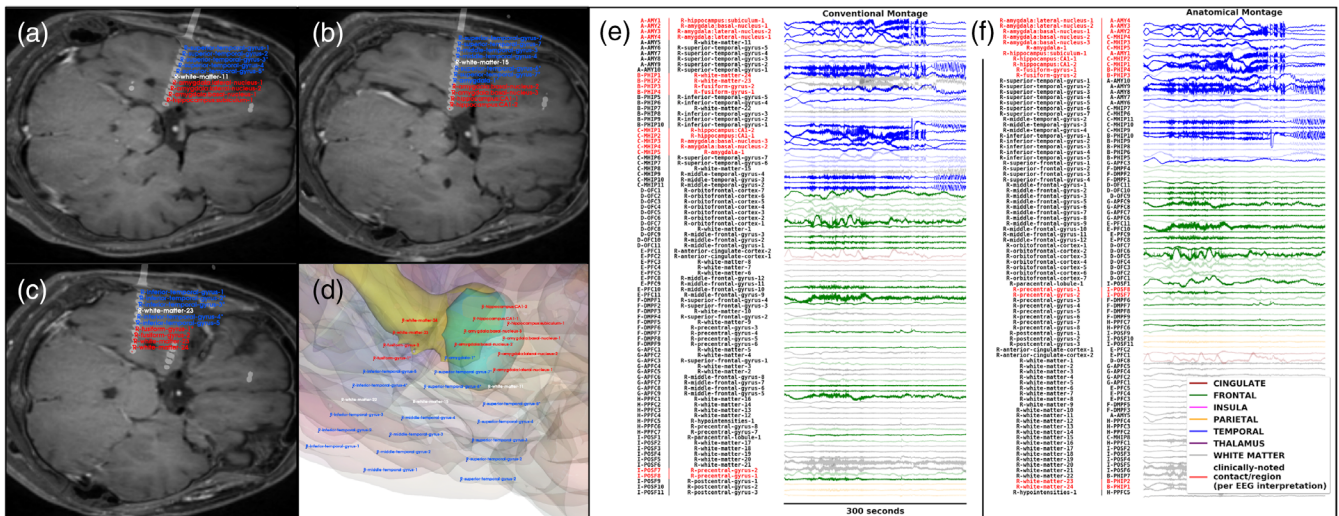
FIGURE 3 Demonstration and comparison of the anatomical versus traditional framework for a unilateral SEEG exploration with temporal lobe onset seizures (subject 1). (a) In a semi-axial view*, an electrode targeting the right medial temporal lobe (MTL) shown on co-registered CT-MRI had deep contacts reside within the amygdala and superficial ones within the lateral temporal lobe, specifically the superior temporal gyrus or the adjacent white matter. Deep contacts were involved in the seizure network (red) and all fell within the MTL. (b) A second electrode targeting the hippocampus also had both the deep and superficial contacts share anatomical groups with the adjacent electrode. (c) Likewise, deep contacts on a third electrode targeting the posterior hippocampus were re-assigned to an anatomical region encompassing multiple contacts residing in the MTL that were involved in the seizure network. (d) A close-up 3D model of the right temporal lobe shows an alternative perspective for viewing the spatial relationships between electrodes. (e) In a 5 min montage containing a clinical seizure, contacts noted to demonstrate significant ictal activity and that were spatially close on the described imaging were separated since conventional montages are constrained by the geometry of physical leads. (f) In the anatomical montage, those contacts collapsed into a contiguous group and the early temporal onset with possible spread to the frontal lobe was even more apparent, as white matter contacts were pruned from the traditional montage. Additionally, a pair of clinically noted contacts targeting the posterior frontal cortex were assigned to the precentral gyrus. Here and in the following figures, labels highlighted in red denote contacts or electrode regions noted to be involved in the seizure network based on clinical EEG interpretation. Recordings from leads localized to white matter but within 2 mm of the assigned gray matter structure are indicated by asterisks (*) on imaging by lighter color shading in montages. *For the electrodes of interest, co-registered CT-MRI reconstructions were transformed to be co-planar with the electrode for visualization purposes.

abnormalities but no scalp correlate to her brief asymmetric tonic seizures, was implanted with broad bilateral coverage across multiple lobes that were notably fragmented on the traditional montage (Figure 5). When translated to the anatomical montage, the frontal, temporal, parietal, and thalamic electrodes were discriminated, with clinically noted seizure nodes emerging along either side of the central sulcus, within the Perisylvian polymicrogyria. Both of these nodes combined deep contacts from electrodes (L-PAR, L-INSU, L-PSYL) that were disparate on the conventional clinical montage. These findings for Subject 3 were used to infer that the electrodes were within the network of the seizure (i.e., the epileptogenic region) but not the seizure onset zone.

For each of the three processed seizure recordings, the distribution of signal correlations of contacts within the same electrode and the same anatomical region with the average signal within each were compared (Figure 6). The neurophysiologic signals, which were bipolar referenced by electrode, were more highly correlated to the group-averaged signal in the anatomical montage than in the traditional lead-based montage. This trend was statistically significant for all three subjects ($p < .01$; two-tailed t-test for differences in means) as well as for the aggregated comparisons ($p < .0001$; two-tailed t-test).

4 | DISCUSSION

We offer a hierarchical labeling of SEEG contacts that is based on precise postoperative location of depth electrode contact within patient-specific anatomy. There have been multiple tools and pipelines developed for localization of depth electrodes in the context of SEEG using some or all of the same software reported here (Davis et al., 2021; Medina Villalon et al., 2018; Narizzano et al., 2017; Princich et al., 2013; Qin et al., 2017; Taylor et al., 2021). Each has its own advantages, such as speed and efficiency, extent of clinical validation, and detailed considerations such as accounting for electrode curve. Yet in addition to limited adoption, previously reported methods persistently remain constrained to the initial contact labels extended from physical leads. Therefore, they fail to leverage the potential to reorganize electrodes anatomically. The primary advantage of our approach is that it begets an intuitive shift in perspective from preoperative target-centered labels to anatomically-based hierarchical ones.

Further, our schema is similar to the clinical approach for interpreting seizures on scalp (Tanaka et al., 2018) and subdural EEG studies (Blume et al., 2001; Devinsky et al., 1989). For those investigations, there is an anatomic spatial arrangement used to evaluate seizures in context of their physiologic field. The spread of discharges
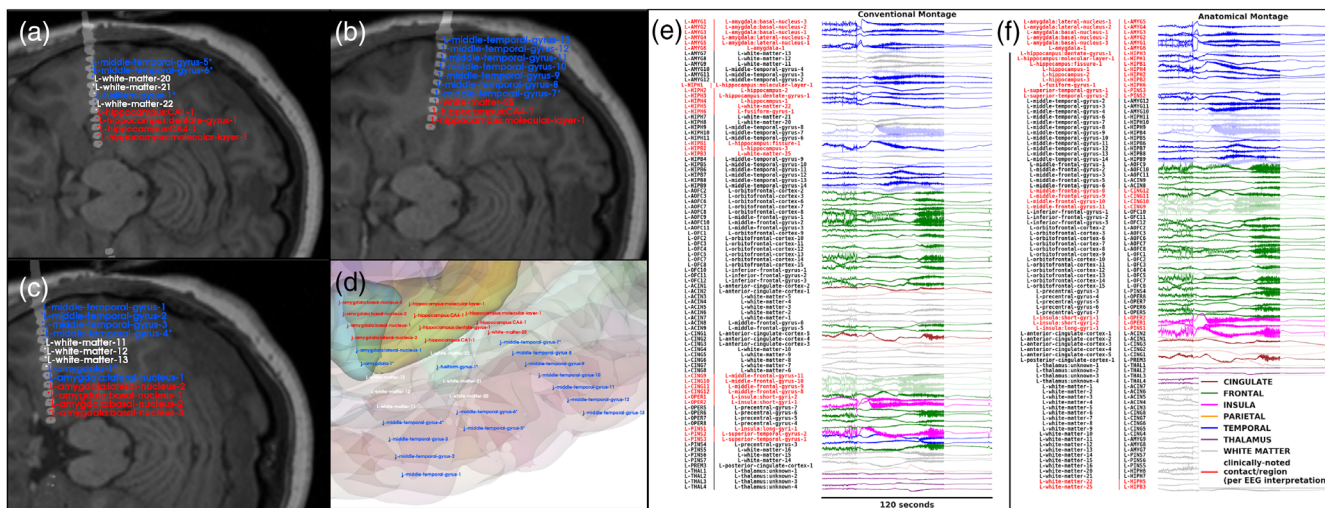
FIGURE 4 Demonstration of the anatomical framework for a subject suffering from seizures with temporal lobe onset and secondary generalization from a complex bilateral SEEG case (subject 2)*. There were three left MTL electrodes targeting the (a) hippocampal head, (b) hippocampal body, and (c) amygdala. Each was comprised of (i) a deep segment within the amygdala or hippocampus that was involved in the clinical seizure, (ii) an intermediate segment of white matter contacts, and (iii) a superficial group of contacts within the middle temporal gyrus. (d) A 3D model of the electrodes in panels a–c sampling the left temporal lobe further illustrates the spatial relationship of the medial versus lateral contacts. (e) In the electrophysiological montages, a clinical seizure begins before the 1-min mark of this 2 min section of recording. There were multiple electrode regions involved in the onset and generalization of the seizure, spanning amygdaloid, hippocampal, cingulate, and insular electrodes. (f) Deep contacts from electrodes targeting the MTL were clustered along with deep contacts from insular and opercular electrodes, demonstrating true locations within the amygdala, hippocampus, as well as more laterally in the superior temporal gyrus and short insular gyrus. Additionally, a second smaller cluster of clinically noted contacts in the insula was revealed as well as a set targeting the cingulate within white matter tracts in close spatial proximity to the middle frontal gyrus. *Only left-sided electrodes are included in these montages for simplicity. All color coding follows the legend in panel f.
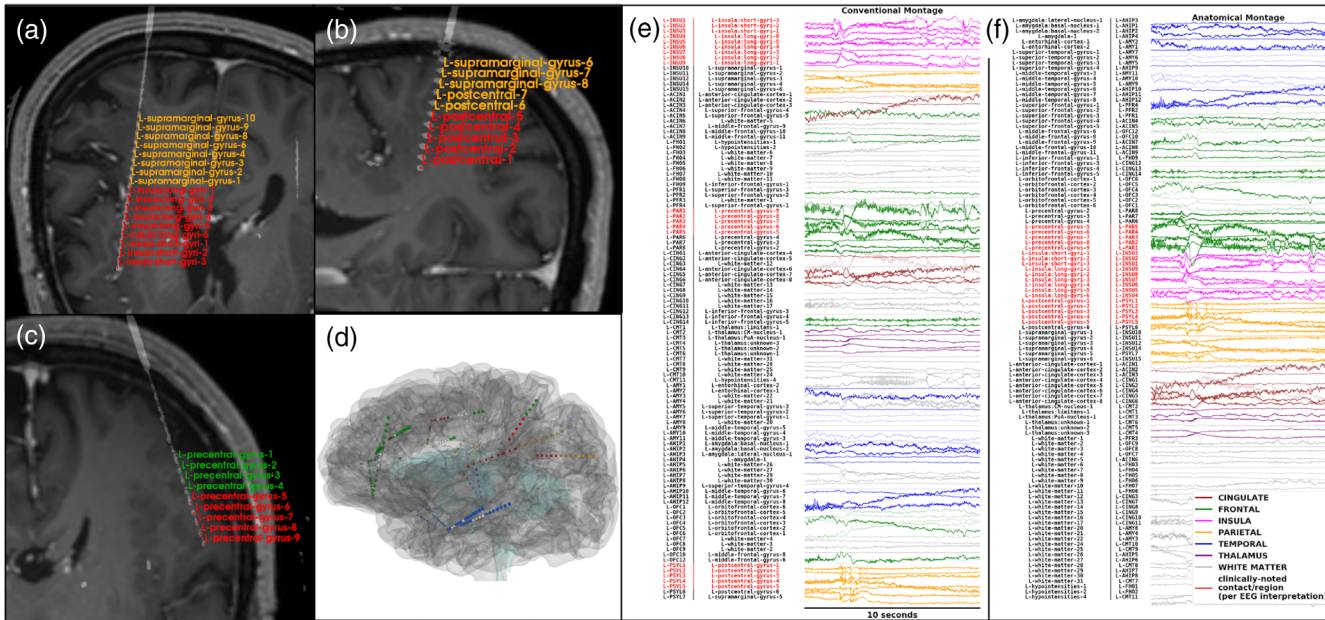

FIGURE 5 Demonstration of the anatomical framework for an SEEG exploration with atypical anatomy and a Perisylvian seizure network (subject 3). (a) An electrode (L-INSU) with a posterior trajectory targeting the left insula contained several deep contacts truly within the insula and sampling a region of cortical microgyria. (b) On this semi-coronal slice viewing an electrode targeting the parietal cortex, the relabeled electrode emphasizes its placement along the left precentral gyrus. (c) Similarly, a third electrode contained contacts sampling the postcentral gyrus. Notably, clinical seizures from this subject were brief and electrographically subtle, with ictal onset of a large direct current shift followed by low voltage fast activity in L-PAR and L-INSU. (d) A 3D reconstruction of contacts was broadly color-coded by lobe instead of electrode, again following the legend in panel f. Note the cluster of bright red contacts in the frontoparietal region, comprising sections of three separate electrodes, that illustrate how this specific exploration sampled the seizure network. On the traditional montage (e), frontal and parietal lobe contacts were intertwined in the traditional montage, whereas the on the anatomical montage (f), these contacts are clustered together. As a result, at least two seizure nodes emerged on either side of the central sulcus, following the Perisylvian polymicrogyria. As with subject 2, only left-sided electrodes are shown for simplicity and because only left-sided electrodes were noted to be involved in the seizure network.
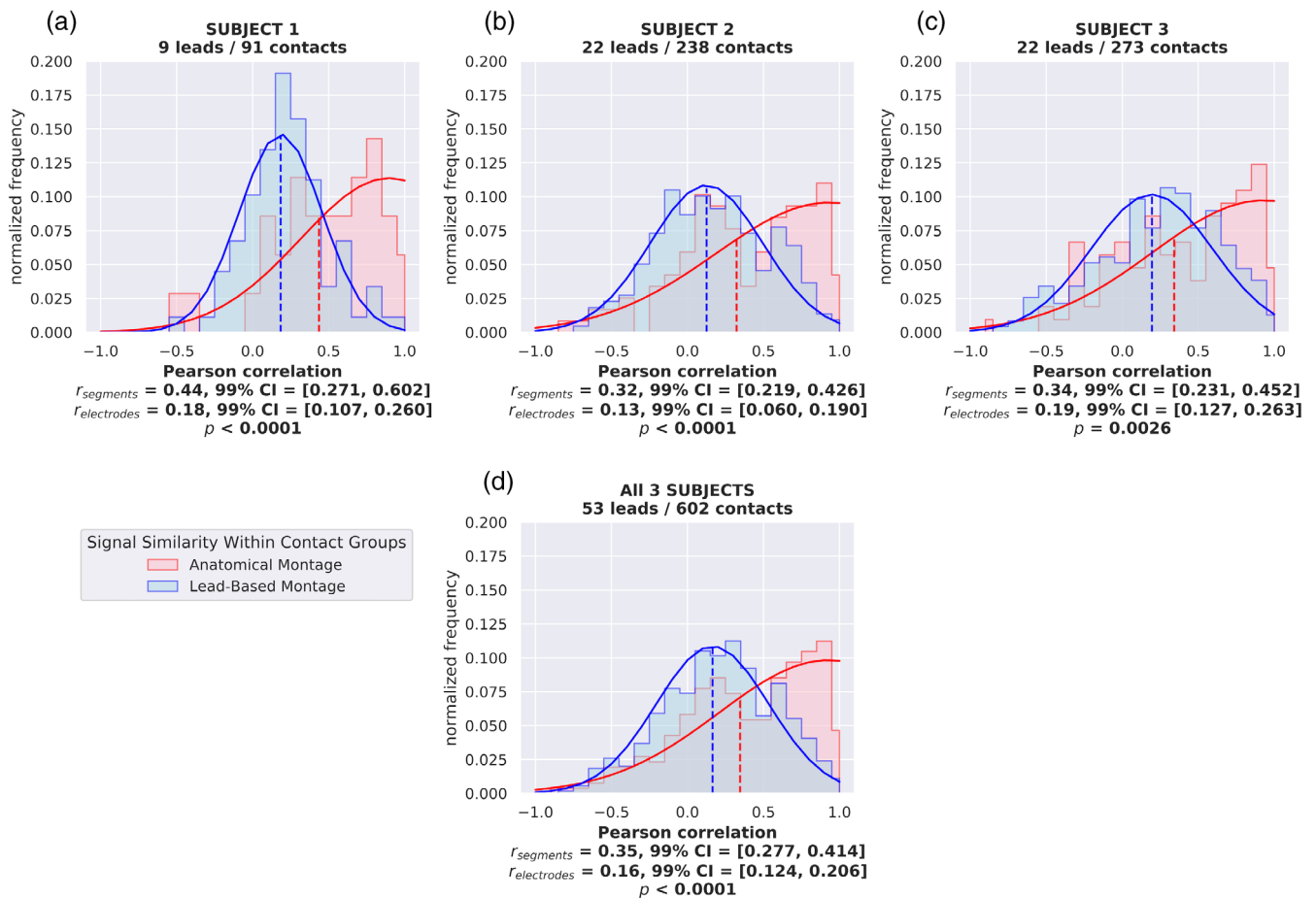
FIGURE 6 Comparison of neurophysiological correlation distributions between the traditional and anatomical montages across three subjects. In general, signals within each electrode were only weakly correlated with the group-averaged signal ($r < 0.3$) while anatomically clustered signals were moderately correlated based on Pearson product–moment correlation ($r > 0.3$). (a) Subject 1 had nine total leads over a unilateral exploration, with the anatomical montage demonstrating a significantly greater average signal similarity within regions versus electrodes. (b) The anatomical montage also offered significantly greater signal correlations within regions for subject 2, who underwent a relatively complex 22-lead exploration of the frontal and temporal lobes in both hemispheres. (c) Subject 3 also had 22 leads in a bilateral exploration, with signals organized by the anatomical montage again demonstrating statistically greater correlation to the group signal. (d) When data were aggregated across all three subjects encompassing 53 total leads, the average signal correlations from anatomically grouped contacts were significantly greater compared to electrode-based groupings. Distributions were fitted to a normal or skew normal distribution for visualization, with mean values denoted by dotted vertical lines.

and seizures is more easily seen across the involved contacts. Our method extends this concept by placing SEEG electrodes, which may encompass a diverse range of trajectories, into a similar anatomic framework to better identify the epileptogenic zone. Indeed, each of the presented examples used to demonstrate its applicability was uniquely complex, as is to be expected for most SEEG explorations. Their typical seizures varied greatly in features including origin, duration, spread, correlation with imaging, and extent to which the seizure onset was captured by lead placement. Given these vast differences that can exist between SEEG investigations, this flexible anatomic approach would greatly standardize the interpretation and communication of data between surgical epilepsy teams.

To date, a practical integrated tool for SEEG contact localization has not yet been accepted clinically. The first report of efficient depth electrode localization using similar software cited access to specialized

personnel as an obstacle toward widespread usage (Medina Villalon et al., 2018; Narizzano et al., 2017; Princich et al., 2013). As an illustration of this issue, the *3DSlicer* software we used is a popular application for research. Custom SEEG packages have been written for it, but still demand familiarity with the environment and require constant maintenance in order to update dependencies. Our institution overcame this problem by uploading clinically useful outputs to the EMR PACS for our patients, which has not yet been reported or accepted as a common step in the clinical course. This final step crucially and durably brings all useful data to the interpreting epileptologists and other end-users within a pre-existing imaging platform.

Notably, EEG technologists often depend on the traditional labeling scheme to generate informative montages of the neurophysiologic recordings. Common referencing schemes for clinical or task-related purposes include bipolar, average, and Laplacian referencing (Li

et al., 2018). Clearly the original nomenclature and reading framework should not be completely abandoned and holds valuable information with regards to signal processing and hardware troubleshooting. Institutions, including our own, may understandably maintain the presentation of clinical electrophysiological information. However, re-referencing electrode clusters based on our proposed scheme can provide additional supplementary information in epileptogenic zone localization. For example, an average montage is still reasonable if electrode-based groupings are replaced with anatomical regions of interest and may be advantageous from a source localization perspective. This possible functionality must also be integrated into popular clinical neurophysiology systems. Further work investigating anatomy-based referencing is necessary to determine if it provides clinically significant novel information or improved signal quality.

4.1 | Limitations

Most methods that automatically segment electrodes rely on cortical maps that either register a standard atlas to the patient MRI or use surface-based parcellation to generate regions. We use the latter approach, though both generally assume normal patient anatomy and can therefore lose fidelity in cases of atypical imaging findings. This issue must be taken heavily into consideration given that patients suffering from epilepsy have a higher rate of these abnormalities, either congenital or acquired, and that such features may be part of the epileptogenic region (Abdel Razek et al., 2009). Of the presented cases, the MRI from Subject 3 demonstrated Perisylvian polymicrogyria that adversely affected the cortical segmentation in the region of the left central sulcus and insula. Since even state-of-the-art image processing software cannot anticipate every edge case, manual segmentation may often be necessary for specific subregions and was performed in the area of this cortical malformation.

5 | CONCLUSION

We offer a novel, generalizable labeling strategy for SEEG that is hierarchical and based on patient-specific anatomy. The spatial and neurophysiologic similarity of signals was greater when presented on our anatomical montage. By including our methods into the existing clinical course, neurophysiologists may adopt a more intuitive perspective for characterizing seizure networks.

CONFLICT OF INTEREST

The authors have declared no conflicts of interest for this article.

ORCID

Bryan Zheng [ID] https://orcid.org/0000-0002-7846-8389

REFERENCES

Abdel Razek, A. A., Kandell, A. Y., Elsorogy, L. G., Elmongy, A., & Basett, A. A. (2009). Disorders of cortical formation: MR imaging features. *American Journal of Neuroradiology*, 30(1), 4–11. https://doi.org/10.3174/ajnr.A1223

Blume, W. T., Ociepa, D., & Kander, V. (2001). Frontal lobe seizure propagation: Scalp and subdural EEG studies. *Epilepsia*, 42(4), 491–503. https://doi.org/10.1046/j.1528-1157.2001.26700.x

Bourdillon, P., Chatillon, C. E., Moles, A., Rheims, S., Catenoix, H., Montavont, A., Ostrowsky-Coste, K., Boulogne, S., Isnard, J., & Guénot, M. (2018). Effective accuracy of stereoelectroencephalography: Robotic 3D versus Talairach orthogonal approaches. *Journal of Neurosurgery*, 131(6), 1938–1946. https://doi.org/10.3171/2018.7.JNS181164

Davis, T. S., Caston, R. M., Philip, B., Charlebois, C. M., Anderson, D. N., Weaver, K. E., Smith, E. H., & Rolston, J. D. (2021). LeGUI: A fast and accurate graphical user Interface for automated detection and anatomical localization of intracranial electrodes. *Frontiers in Neuroscience*, 15, 769872. https://doi.org/10.3389/fnins.2021.769872

Desikan, R. S., Segonne, F., Fischl, B., Quinn, B. T., Dickerson, B. C., Blacker, D., Buckner, R. L., Dale, A. M., Maguire, R. P., Hyman, B. T., Albert, M. S., & Killiany, R. J. (2006). An automated labeling system for subdividing the human cerebral cortex on MRI scans into gyral based regions of interest. *NeuroImage*, 31(3), 968–980. https://doi.org/10.1016/j.neuroimage.2006.01.021

Destrieux, C., Fischl, B., Dale, A., & Halgren, E. (2010). Automatic parcellation of human cortical gyri and sulci using standard anatomical nomenclature. *NeuroImage*, 53(1), 1–15. https://doi.org/10.1016/j.neuroimage.2010.06.010

Devinsky, O., Sato, S., Kufta, C. V., Ito, B., Rose, D. F., Theodore, W. H., & Porter, R. J. (1989). Electroencephalographic studies of simple partial seizures with subdural electrode recordings. *Neurology*, 39(4), 527–533. https://doi.org/10.1212/wnl.39.4.527

Diehl, B., & Luders, H. O. (2000). Temporal lobe epilepsy: When are invasive recordings needed? *Epilepsia*, 41(Suppl 3), S61–S74. https://doi.org/10.1111/j.1528-1157.2000.tb01536.x

Englot, D. J., Breshears, J. D., Sun, P. P., Chang, E. F., & Auguste, K. I. (2013). Seizure outcomes after resective surgery for extra-temporal lobe epilepsy in pediatric patients. *Journal of Neurosurgery. Pediatrics*, 12(2), 126–133. https://doi.org/10.3171/2013.5.PEDS1336

Englot, D. J., Wang, D. D., Rolston, J. D., Shih, T. T., & Chang, E. F. (2012). Rates and predictors of long-term seizure freedom after frontal lobe epilepsy surgery: A systematic review and meta-analysis. *Journal of Neurosurgery*, 116(5), 1042–1048. https://doi.org/10.3171/2012.1.JNS111620

Faraji, A. H., Remick, M., & Abel, T. J. (2020). Contributions of robotics to the safety and efficacy of invasive monitoring with Stereoelectroencephalography. *Frontiers in Neurology*, 11, 570010. https://doi.org/10.3389/fneur.2020.570010

Fedorov, A., Beichel, R., Kalpathy-Cramer, J., Finet, J., Fillion-Robin, J. C., Pujol, S., Bauer, C., Jennings, D., Fennessy, F., Sonka, M., Buatti, J., Aylward, S., Miller, J. V., Pieper, S., & Kikinis, R. (2012). 3D slicer as an image computing platform for the quantitative imaging network. *Magnetic Resonance Imaging*, 30(9), 1323–1341. https://doi.org/10.1016/j.mri.2012.05.001

Fischl, B., van der Kouwe, A., Destrieux, C., Halgren, E., Ségonne, F., Salat, D. H., Busa, E., Seidman, L. J., Goldstein, J., Kennedy, D.,

Caviness, V., Makris, N., Rosen, B., & Dale, A. M. (2004). Automatically parcellating the human cerebral cortex. *Cerebral Cortex*, *14*(1), 11–22. https://doi.org/10.1093/cercor/bhg087

GBD 2016 Brain and Other CNS Cancer Collaborators. (2019). Global, regional, and national burden of brain and other CNS cancer, 1990–2016: A systematic analysis for the global burden of disease study 2016. *Lancet Neurology*, *18*(4), 376–393. https://doi.org/10.1016/S1474-4422(18)30468-X

Iglesias, J. E., Augustinack, J. C., Nguyen, K., Player, C. M., Player, A., Wright, M., Roy, N., Frosch, M. P., McKee, A., Wald, L. L., Fischl, B., van Leemput, K., & Alzheimer's Disease Neuroimaging Initiative. (2015). A computational atlas of the hippocampal formation using ex vivo, ultra-high resolution MRI: Application to adaptive segmentation of in vivo MRI. *NeuroImage*, *115*, 117–137. https://doi.org/10.1016/j.neuroimage.2015.04.042

Iglesias, J. E., Insausti, R., Lerma-Usabiaga, G., Bocchetta, M., van Leemput, K., Greve, D. N., van der Kouwe, A., Alzheimer's Disease Neuroimaging Initiative, Fischl, B., Caballero-Gaudes, C., & Paz-Alonso, P. M. (2018). A probabilistic atlas of the human thalamic nuclei combining ex vivo MRI and histology. *NeuroImage*, *183*, 314–326. https://doi.org/10.1016/j.neuroimage.2018.08.012

Iglesias, J. E., van Leemput, K., Augustinack, J., Insausti, R., Fischl, B., Reuter, M., & Alzheimer's Disease Neuroimaging Initiative. (2016). Bayesian longitudinal segmentation of hippocampal substructures in brain MRI using subject-specific atlases. *NeuroImage*, *141*, 542–555. https://doi.org/10.1016/j.neuroimage.2016.07.020

Jobst, B. C., & Cascino, G. D. (2015). Resective epilepsy surgery for drug-resistant focal epilepsy: A review. *JAMA*, *313*(3), 285–293. https://doi.org/10.1001/jama.2014.17426

Jung, B., Taylor, P. A., Seidlitz, J., Sponheim, C., Perkins, P., Ungerleider, L. G., Glen, D., & Messinger, A. (2021). A comprehensive macaque fMRI pipeline and hierarchical atlas. *NeuroImage*, *235*, 117997. https://doi.org/10.1016/j.neuroimage.2021.117997

Khoo, H. M., Hall, J. A., Dubeau, F., Tani, N., Oshino, S., Fujita, Y., Gotman, J., & Kishima, H. (2020). Technical aspects of SEEG and its interpretation in the delineation of the epileptogenic zone. *Neurologia Medico-Chirurgica (Tokyo)*, *60*(12), 565–580. https://doi.org/10.2176/nmc.st.2020-0176

Kwan, P., & Brodie, M. J. (2000). Early identification of refractory epilepsy. *The New England Journal of Medicine*, *342*(5), 314–319. https://doi.org/10.1056/NEJM200002033420503

Li, G., Jiang, S., Paraskevopoulou, S. E., Wang, M., Xu, Y., Wu, Z., Chen, L., Zhang, D., & Schalk, G. (2018). Optimal referencing for stereo-electroencephalographic (SEEG) recordings. *NeuroImage*, *183*, 327–335. https://doi.org/10.1016/j.neuroimage.2018.08.020

Medina Villalon, S., Paz, R., Roehri, N., Lagarde, S., Pizzo, F., Colombet, B., Bartolomei, F., Carron, R., & Bénar, C. G. (2018). EpiTools, a software suite for presurgical brain mapping in epilepsy: Intracerebral EEG. *Journal of Neuroscience Methods*, *303*, 7–15. https://doi.org/10.1016/j.jneumeth.2018.03.018

Mullin, J. P., Shriver, M., Alomar, S., Najm, I., Bulacio, J., Chauvel, P., & Gonzalez-Martinez, J. (2016). Is SEEG safe? A systematic review and meta-analysis of stereo-electroencephalography-related complications. *Epilepsia*, *57*(3), 386–401. https://doi.org/10.1111/epi.13298

Narizzano, M., Arnulfo, G., Ricci, S., Toselli, B., Tisdall, M., Canessa, A., Fato, M. M., & Cardinale, F. (2017). SEEG assistant: A 3DSlicer extension to support epilepsy surgery. *BMC Bioinformatics*, *18*(1), 124. https://doi.org/10.1186/s12859-017-1545-8

Picot, M. C., Baldy-Moulinier, M., Daures, J. P., Dujols, P., & Crespel, A. (2008). The prevalence of epilepsy and pharmacoresistant epilepsy in adults: A population-based study in a Western European country. *Epilepsia*, *49*(7), 1230–1238. https://doi.org/10.1111/j.1528-1167.2008.01579.x

Podkorytova, I., Hoes, K., & Lega, B. (2016). Stereo-encephalography versus subdural electrodes for seizure localization. *Neurosurgery Clinics of North America*, *27*(1), 97–109. https://doi.org/10.1016/j.nec.2015.08.008

Princich, J. P., Wassermann, D., Latini, F., Oddo, S., Blenkmann, A. O., Seifer, G., & Kochen, S. (2013). Rapid and efficient localization of depth electrodes and cortical labeling using free and open source medical software in epilepsy surgery candidates. *Frontiers in Neuroscience*, *7*, 260. https://doi.org/10.3389/fnins.2013.00260

Qin, C., Tan, Z., Pan, Y., Li, Y., Wang, L., Ren, L., Zhou, W., & Wang, L. (2017). Automatic and precise localization and cortical labeling of subdural and depth intracranial electrodes. *Frontiers in Neuroinformatics*, *11*, 10. https://doi.org/10.3389/fninf.2017.00010

Reveley, C., Gruslys, A., Ye, F. Q., Glen, D., Samaha, J., E. Russ, B., Saad, Z., K. Seth, A., Leopold, D. A., & Saleem, K. S. (2017). Three-dimensional digital template atlas of the macaque Brain. *Cerebral Cortex*, *27*(9), 4463–4477. https://doi.org/10.1093/cercor/bhw248

Sander, J. W. (1993). Some aspects of prognosis in the epilepsies: A review. *Epilepsia*, *34*(6), 1007–1016. https://doi.org/10.1111/j.1528-1157.1993.tb02126.x

Sarikaya, I. (2015). PET studies in epilepsy. *American Journal of Nuclear Medicine and Molecular Imaging*, *5*(5), 416–430.

Saygin, Z. M., Kliemann, D., Iglesias, J. E., van der Kouwe, A. J. W., Boyd, E., Reuter, M., Stevens, A., van Leemput, K., McKee, A., Frosch, M. P., Fischl, B., & Augustinack, J. C. (2017). High-resolution magnetic resonance imaging reveals nuclei of the human amygdala: Manual segmentation to automatic atlas. *NeuroImage*, *155*, 370–382. https://doi.org/10.1016/j.neuroimage.2017.04.046

Stone, S., Madsen, J. R., Bolton, J., Pearl, P. L., Chavakula, V., & Day, E. (2020). A standardized electrode nomenclature for Stereoelectroencephalography applications. *Journal of Clinical Neurophysiology*, *38*(6), 509–515. https://doi.org/10.1097/WNP.0000000000000724

Tanaka, H., Khoo, H. M., Dubeau, F., & Gotman, J. (2018). Association between scalp and intracerebral electroencephalographic seizure-onset patterns: A study in different lesional pathological substrates. *Epilepsia*, *59*(2), 420–430. https://doi.org/10.1111/epi.13979

Taussig, D., Chipaux, M., Fohlen, M., Dorison, N., Bekaert, O., Ferrand-Sorbets, S., & Dorfmüller, G. (2020). Invasive evaluation in children (SEEG vs subdural grids). *Seizure*, *77*, 43–51. https://doi.org/10.1016/j.seizure.2018.11.008

Taylor, K. N., Joshi, A. A., Hirfanoglu, T., Grinenko, O., Liu, P., Wang, X., Gonzalez-Martinez, J. A., Leahy, R. M., Mosher, J. C., & Nair, D. R. (2021). Validation of semi-automated anatomically labeled SEEG contacts in a brain atlas for mapping connectivity in focal epilepsy. *Epilepsia Open*, *6*(3), 493–503. https://doi.org/10.1002/epi4.12499